THE JOURNAL OF PHYSICAL CHEMISTRY C
A JOURNAL OF THE AMERICAN CHEMICAL SOCIETY
pubs.acs.org/JPCC Article

A Modified Embedded-Atom Potential for Fe-Cr-Si Alloys

Shiddartha Paul, Mario Muralles, Daniel Schwen, Michael Short, and Kasra Momeni*

Cite This: J. Phys. Chem. C 2021, 125, 22863−22871 Read Online

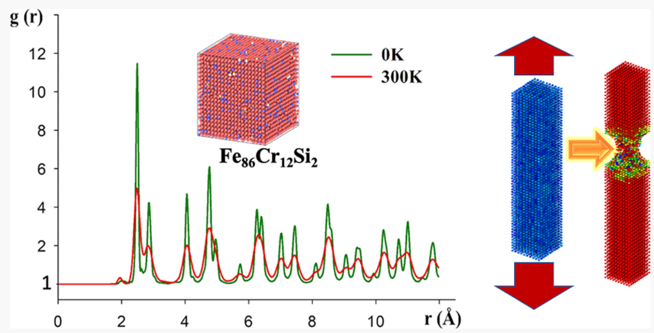

ABSTRACT: We developed a modified embedded atom method (MEAM) potential for Fe-Cr-Si ternary systems. These alloys have superior corrosion and crack resistance, making them candidate materials for several engineering applications such as accident-tolerant fuel cladding. We used a multiobjective optimization approach to match Fe-Cr-Si's elastic constants, ground-state energies, and structural parameters with ab initio calculations. The potential has been parameterized by fitting to a set of literature values obtained using density functional theory (DFT) or experimental studies. The developed potential was used in molecular dynamics (MD) simulations to extract mechanical and thermal properties. We obtained the calculated elastic constants for Fe-Cr-Si binary interactions using the proposed potential, agreeing with ab initio calculations. Our calculated self-diffusion coefficient values and defect formation energy using this potential are in good agreement with the previous literature. Therefore, the developed potential can investigate the fundamental behaviors on an atomic scale under harsh conditions like elevated temperature and irradiation.

1. INTRODUCTION

There is an increasing need for materials that can operate under extreme conditions, specifically elevated temperatures. Iron−chromium (Fe-Cr) alloys are prime candidates with outstanding creep strength and heat resistance, for example, T91.[1,2] We may refer to superheaters in boilers, main steam pipelines, and heating furnace piping in the petrochemical industry as some of their current applications.[3,4] Fe-Cr alloys are also one of the prime candidate materials for nuclear fuel cladding,[5,6] specifically for Generation IV nuclear reactors with a life of 60+ years and operating in temperatures as high as 1000 K and extreme radiation doses because they have higher oxidation resistance compared to zirconium alloys. These emerging needs further emphasize the necessity of computational studies for Fe-Cr alloys, as experimental radiation tests are costly and require a minimum of 7 years of testing.

A 9−12% Cr concentration exhibits increased strength and thermal conductivity while lowering the thermal expansion coefficient.[7] Furthermore, silicon as a common additive to Fe-Cr alloys can significantly impact their final properties by segregating grain boundaries.[8,9] These alloys have already been used as part of multimetallic layered composites (MMLC) for fuel cladding material implementation for accident-tolerant nuclear fuel cladding.[10−12]

Molecular dynamics (MD) is a powerful technique that provides a thorough insight into the atomistic mechanism governing material behaviors. The modified embedded-atom method (MEAM) in its second nearest-neighbor version, called 2NN MEAM interatomic potential,[13−15] is an improved formalism with angular dependence. It can predict phase stability and mechanical behavior for complex systems, such as high entropy alloys (HEA), even under irradiation.[16,17] There is no previous interatomic potential development for Fe-Cr-Si as a ternary system. Nonetheless, a multicomponent system can be described by the addition of its unary and binary interactions. In total, six interactions fully represent the Fe-Cr-Si alloy, three pure element systems plus the Fe-Cr, Fe-Si, and Cr-Si binary systems. Two studies have developed MEAM potentials for HEAs that contain the majority of the required interactions for the Fe-Cr-Si, that is, potentials for Co-Cr-Fe-Mn-Ni and Al-Si-Mg-Cu-Fe alloys.[18,19] Here, we capitalized on unary systems and binary Fe-Cr and Fe-Si interactions from these potentials and developed the MEAM potential for Cr-Si interactions from scratch. The interactions/parameters extracted from each of the references are shown in Table S1 in the Supporting Information.

2. POTENTIAL DEVELOPMENT

2.1. Interatomic Formulation. The 2NN MEAM interatomic potential relies on two parts, the summation of the embedding atom function and the pairwise interactions, as

Received: August 7, 2021
Revised: September 27, 2021
Published: October 6, 2021

https://doi.org/10.1021/acs.jpcc.1c07021
J. Phys. Chem. C 2021, 125, 22863−22871

Table 1. MEAM Potential Parameters for Unary Systems Adopted from Previous Studies[18,19,a]

elem.	E_c	r_e	α	A	$\beta^{(0)}$	$\beta^{(1)}$	$\beta^{(2)}$	$\beta^{(3)}$	$t^{(1)}$	$t^{(2)}$	$t^{(3)}$	C_{min}	C_{max}	d^+	d^-
Fe[b]	4.29	2.48	5.157	0.56	4.15	1.00	1.00	1.00	2.60	1.80	−7.20	0.36	2.80	0.05	0.05
Cr[b]	4.10	2.495	5.580	0.52	6.49	1.00	6.00	1.00	2.00	6.80	−8.00	0.71	2.80	0.02	0.10
Si[c]	4.63	2.39	4.870	1.00	4.40	5.50	5.50	5.50	2.05	4.47	−1.80	2.00	2.80	0.00	0.00

[a]E_c is given in eV, while r_e, $C_{min,}$ and C_{max} are given in Å; the others are unitless. [b]Ref 18. [c]Ref 19.

Table 2. Comparison of Calculated Structural and Elastic Properties for the Adopted Unary Potentials (Shaded) vs Other Studies[a]

	str.	E_c	a_{lat}	C_{11}	C_{12}	C_{44}	B
Fe	BCC						
MEAM[18]		−4.29	2.863	242.17	138.41	121.46	173.00
MEAM[26]		−4.29	2.860	226	140	116	
MEAM[21]				243.00	138.00	121.90	
Exp.[27]				243.10	138.10	121.90	
Cr	BCC						
MEAM[18]		−4.10	2.880	344.45	112.89	130.47	190.08
MEAM[26]		−4.10	2.885	350.00	67.00	100.00	
MEAM[21]				390.90	89.70	103.40	
Exp.[27]				391.00	89.60	103.20	
Si	DIA						
MEAM[19]		−4.63	5.431	163.78	64.54	76.46	97.62
MEAM[28]				164	65	76	
DFT[29]		−4.63	5.429	171.5	67.1	81.1	101.9
DFT[30]				154.6	58.1	74.4	

[a]E_c is given in eV and a_{lat} in Å, while the elastic constants and B are all in GPa.

$$E = \sum_i \left[F_i(\bar{\rho}_i) + \frac{1}{2} \sum_{j \neq i} S_{ij}\phi(R_{ij}) \right] \tag{1}$$

In the first part, a pure mathematical formalism, F_i, represents the embedding function for the background electron density of site i, $\bar{\rho}_i$. In the second part S_{ij} is the screening factor determining the degree of screening to the pairwise interaction ϕ between i and j by the neighboring atoms and is mainly based on the equation of states (EOS).[20] In total, 13 parameters are needed for the energy function (see the Supporting Information). Three of them are usually adopted from experimental or DFT calculations, that is, cohesive energy E_c, equilibrium nearest-neighbor distance r_e, bulk modulus B, and α representing the exponential decay factor. These parameters are used mainly to satisfy the EOS. The rest of the parameters are obtained by fitting the potential, that is, $t^{(1-3)}$ weighting factors for electron density components and $\beta^{(0-3)}$ the exponential decay factors. A represents an embedding energy scaling factor and d the pressure derivative of bulk modulus; the latter can be adjusted to influence the attractive or repulsive interactions, d^+, and d^-, respectively. Finally, we have the many-body screening parameters C_{min}/C_{max}.

Regarding multibody interactions, the MEAM captures the directional bonding using the C_{min} and C_{max} parameters, representing the limits of the screening region. There are eight screening parameters in total that depend on their direction. For a binary alloy, the screening can be in four directions (*A, A, B*), (*B, B,A*), (*A,B,A*), and (*A,B,B*), where *A* and *B* represent the atoms of each element. The complete MEAM theory has been widely discussed elsewhere.[13,21,22]

2.2. Unary Parameters. We adopted all unary parameters from previous publications.[18,19] The selected potential parameters for Fe, Cr, and Si are presented in Table 1. The first step to build the interatomic potential for the ternary alloy is to check the reproducibility of the unary force fields. We performed MD calculations by minimizing the force and energy of the Fe, Cr, and Si unit cells at 0 K using the conjugate gradient (CG) technique[23] incorporated in the large-scale atomic/molecular massively parallel simulator (LAMMPS).[24]

Table 2 shows the resultant ground states. Here, we compare different material properties—including the cohesive energy, E_c, the lattice constant, a, elastic constants (C_{11}, C_{12}, and C_{14}), and bulk modulus, B—to the values reported in the literature. In Fe and Cr, the reference structure was defined as body-centered cubic (BCC), while for Si, it was the diamond structure (DIA). Our calculations for Fe and Si reproduced the MEAM-adopted references in agreement with experiments and other computational calculations. The Cr potential reproduced our main reference calculations. However, some deviations are present when compared with experimental and other MEAM calculations. The developers acknowledged these deviations in their publication[18] and claimed to be necessary to induce phase stability in other binary interactions.

2.3. Binary and Ternary Parameterization. After validating the parameters for the unary systems, the next step is to parameterize the binary alloys. In total, three binary interactions define the complete ternary system, Fe-Cr, Fe-Si, and Cr-Si. The Fe-Cr and Fe-Si parameters are already defined. Nonetheless, the Fe-Si interactions were fitted to a different iron alloy, and therefore refitting was necessary. Furthermore, MEAM parameterization for the Cr-Si system is still lacking. Thus, the best path forward is developing a potential that can reproduce the mechanical and structural aspects of the Cr-Si alloy. We implemented a multiobjective optimization (MOO) for the fitting procedure, as described in the literature.[25] Here,

Table 3. MEAM Potential Parameters for Binary Systems[a]

system	E_c	r_e	α	d^+	d^-	$\rho 0$	C_{min} (A,A,B)	C_{min} (B,B,A)	C_{min} (A,B,A)	C_{min} (A,B,B)	C_{max} (A,A,B)	C_{max} (B,B,A)	C_{max} (A,B,A)	C_{max} (A,B,B)
Fe-Cr	4.10	2.487	5.43	0.035	0.075	1.0	0.36	0.71	0.52	0.52	2.8	2.8	2.8	2.8
Fe-Si	5.50	2.4	4.90	0.1	0.1	1.0	1.20	2.20	0.8	1.8	2.8	2.5	2.5	2.2
Cr-Si	10.27	2.6	4.81	0.52	0.03	1.0	1.02	1.57	2.0	2.0	2.8	2.8	2.8	2.8

[a] E_c is given in eV, r_e, C_{min}, and C_{max} in Å; the others are unitless.

we extracted the initial E_c, r_e, and B from DFT calculations.[18,19] We did not consider the two global adjusting parameters in this training, for example, the cut-off radius and the length of smoothing distance because they would affect the rest of binary interactions. Priority was given to the global parameter set by the Fe-Cr interaction because we aim at studying Fe-Cr-Si alloys with low Si concentrations.

In this study, the primary reference structure for Fe-Si was defined as Cs-Cl, that is, the B2 structure. There are also reports on Fe-Si with B2 and Na-Cl-like B1 structures and an experimentally observed B20, featuring a relatively low internal symmetry.[19,31−33] However, the reported results are not consistent and present significant discrepancies. Thus, we decided to adopt the B2 (ordered BCC) structure because the Fe-Cr-Si system with a low Si content is known to array in a BCC structure.

The Cr-Si equiatomic interactions are described to form a $P2_13$ cubic phase with low symmetry similar to the B20 structure of the Fe-Si alloy.[34] Potential fitting is a tedious and time-consuming process because of the many possible combinations and the complex behavior of the many-body systems that eventually work in many cases.[25] To reduce the time spent for developing the potential, first, we identified the dominant screening parameters and how they affect the results. The binary unit cells were minimized using the same method as for the unary systems. Afterward, the system stress tensors, as well as energetic and structural properties, were measured. Following the MOO procedure, weights were assigned to the outputs to maintain a well-balanced potential focused on reproducing the ground-state energies, elastic constants, and structural parameters. The present calculation overestimates the reference E_c for the Cr-Si alloy to ensure a sound balance output without modifying the unary systems. The Fe-Cr-adopted parameters, as well as the Fe-Si and Cr-Si-fitted parameters, are shown in Table 3. The resulting calculations for the equiatomic compositions are compared with various studies in Table 4.

Ternary interactions require six new parameters, three C_{min} and three C_{max}. These parameters are obtained using an averaging approach over the binary parameters. Here, the screening of a C atom in the interaction between A and B atoms [C_{min}/C_{max} (A, C, B)] is an average between the degree of screening by the C atom to the A-A [C_{min}/C_{max} (A, C, A)] and B-B [C_{min}/C_{max} (B, C, B)] interactions. The obtained values of these averages are listed in Table 5.

The Fe-Si interactions represent a challenge to study, given the discrepancies in the elastic and structural results obtained by the references.[19,31−33,35] Our calculations for the B2 structure show stiffness constants inside the range set by first-principles calculations but with a slightly lower lattice constant. The ternary potential exhibited discrepancies when calculating Fe-Si B20 properties, showing a much lower lattice constant and overestimating C_{11} and C_{12}. However, the potential maintained the trend shown by all the references, for example, B2 presents a $C_{11} > C_{12} > C_{44}$ relationship while B20 presents $C_{11} > C_{44} > C_{12}$.

Table 4. Comparison of the Calculated Structural and Elastic Properties of the Equiatomic Binary Interactions Described by the Developed Potential (Shaded) vs Other Studies[a]

	str.	E_c	a_{lat}	C_{11}	C_{12}	C_{44}	B
Fe-Cr	**B2**	−4.31	2.80	348	115	88	193
DFT[38]				350	150	124	219
DFT GGA[39]			2.86			98	197
Fe-Si	**B2**	−4.97	2.62	480	141	100	254
MEAM[19]						36	177
DFT GGA[19]						87	231
DFT LDA[31]			2.70	510	160	135	262
DFT GGA[31]			2.77	435	125	95	220
DFT LDA[33]			2.72	460	173	114	269
DFT GGA[35]			2.77				221
	B20	−6.61	4.02	377	211	299	267
DFT GGA[9]							226
DFT LDA[21]			4.83	440	150	190	255
DFT GGA[21]			4.48	385	120	160	221
DFT LDA[35]		−6.58	4.38				257
DFT GGA[35]		−5.33	4.42				209
Exp.[32]			4.48	345	106	138	
Cr-Si	**B20**	−7.98	4.58	398	103	121	201
DFT[36]		−8.13	4.59	390	112	125	205
exp. (100 K)[37]							150

[a] E_c is given in eV, a_{lat} in Å, the elastic constants, and moduli are all in GPa.

Table 5. MEAM Potential Parameters for the Ternary System[a]

screening direction	parameter
C_{min} (Fe-Cr-Si)	0.86 $([0.5(C_{min}{}^{Fe\text{-}Cr\text{-}Fe})^{1/2} + 0.5(C_{min}{}^{Si\text{-}Cr\text{-}Si})^{1/2}]^2)$
C_{min} (Cr-Fe-Si)	0.93 $([0.5(C_{min}{}^{Cr\text{-}Fe\text{-}Cr})^{1/2} + 0.5(C_{min}{}^{Si\text{-}Fe\text{-}Si})^{1/2}]^2)$
C_{min} (Cr-Si-Fe)	1.55 $([0.5(C_{min}{}^{Cr\text{-}Si\text{-}Cr})^{1/2} + 0.5(C_{min}{}^{Fe\text{-}Si\text{-}Fe})^{1/2}]^2)$
C_{max} (Fe-Cr-Si)	2.80 $([0.5(C_{max}{}^{Fe\text{-}Cr\text{-}Fe})^{1/2} + 0.5(C_{max}{}^{Si\text{-}Cr\text{-}Si})^{1/2}]^2)$
C_{max} (Cr-Fe-Si)	2.80 $([0.5(C_{max}{}^{Cr\text{-}Fe\text{-}Cr})^{1/2} + 0.5(C_{max}{}^{Si\text{-}Fe\text{-}Si})^{1/2}]^2)$
C_{max} (Cr-Si-Fe)	2.64 $[0.5(C_{max}{}^{Cr\text{-}Si\text{-}Cr})^{1/2} + 0.5(C_{max}{}^{Fe\text{-}Si\text{-}Fe})^{1/2}]^2)$

[a] C_{min}/C_{max} are given in Å.

There is a mismatch between the bulk moduli of the equiatomic Cr-Si system calculated using DFT[36] and what is measured experimentally.[37] This discrepancy is mainly related to thermal effects because the experiment was performed at different temperatures starting at 100 K. Nonetheless, the experiment shows an inverse relationship between temperature and bulk modulus, meaning that a closer value is expected at 0 K.

The fitted Cr-Si potential shows a good agreement with DFT calculations. The maximum deviation obtained was ~7% for the elastic constant C_{12}, maintaining a reasonable proportionality with the rest of the parameters. The obtained

https://doi.org/10.1021/acs.jpcc.1c07021
J. Phys. Chem. C 2021, 125, 22863−22871

Table 6. Structural and Elastic Properties for Nonequiatomic Fe-Si and Cr-Si Compounds Described by the Developed Potential (Shaded) vs Other Studies[a]

	comp.	space group	system	method	a_{lat}	b_{lat}	c_{lat}	B
Fe-Si	**Fe_3Si**	***Fm-3 m***	**cubic**		2.17			169
				DFT[19]	2.22			204
				MEAM[19]	2.29			163
	Fe_2Si	***P-3 m1***	**trigonal**		3.92		4.83	243
				DFT[42]	3.92		4.84	237
				DFT[43]	(c/a = 1.24)			240
				Exp.[43]	(c/a = 1.25)			
	$FeSi_2$	***P4/mmm***	**tetragonal**		2.55		5.18	187
				DFT[42]	2.70		5.13	183
				MEAM[19]				170
Cr-Si	**Cr_3Si**	***Pm-3n***	**cubic**		4.62			253
				DFT[36]	4.51			251
				DFT[41]	4.51			242
				Exp.[44]	4.56			
	Cr_5Si_3	***I4/mcm***	**tetragonal**		4.67		9.76	180
				DFT[36]	4.58		9.06	221
				DFT[41]				221
				Exp.[45]	4.63		9.16	
	$CrSi_2$	***$P6_222$***	**hexagonal**		4.70		6.76	167
				DFT[36]	4.39		6.36	196
				DFT[46]	4.36		6.32	216

[a]The lattices a_{lat}, b_{lat}, and c_{lat} are given in Å and the bulk modulus B in GPa.

binding energy is slightly higher, that is, by 0.15 eV, but it was a necessary trade-off to obtain a satisfactory agreement on the mechanical and structural properties.

Nonequiatomic compounds are metastable in the literature.[40] In this study, we assessed the capabilities of the potential to stabilize some of these structures. The compounds explored are Fe_3Si, Fe_2Si, and $FeSi_2$ for the Fe-Si interactions and Cr_3Si, Cr_5Si_3, and $CrSi_2$ for the Cr-Si interactions. The results are presented in Table 6. As stated, the Fe-Cr interaction has been completely adopted in this work, and detailed studies can be found in the literature. Thus, other compounds were not included. The results of the tested Fe-Si compounds show good structural and elastic agreement with the studies. The Fe_3Si compound denotes a lower bulk modulus compared with ab initio calculations. However, the obtained bulk modulus for Fe_3Si and $FeSi_2$ is in better agreement than a previously developed Fe-Si MEAM potential,[19] which is also observable for the equiatomic composition. Overall, we found that the developed potential overestimates the size of the lattice parameters for the Cr-Si compounds, showing slightly larger values compared with that in the literature. The Cr3Si compound correctly reproduces the bulk modulus, while Cr_5Si_3 and $CrSi_2$ denote a lower modulus. However, the calculated bulk modulus decreases as the composition becomes more Si-rich, as observed by ab initio calculations.[41]

3. BULK MECHANICAL PROPERTIES

To test the bulk response of the developed ternary potential, we generated the commercial steel $Fe-Cr_{12}-Si_2$, which is widely used for nuclear applications. This alloy features a BCC structure similar to the α-Fe phase because of the high Fe content. Thus, we built a simulation box with 16,000 BCC iron atoms. Randomly selected Fe atoms were substituted with Cr and Si atoms to generate the composition mentioned above. The bulk was minimized in the same style, as described for the unary and binary systems.

Finally, elastic properties such as bulk modulus B, Young modulus E, shear modulus G, and Poisson's ratio ν were calculated using Reuss-Voight equations.[47] The results from our MEAM potential are compared with the reported experimental measurements given in Table 7. Although we captured the general trend, we predicted higher values than the experimentally measured ones.

Table 7. Calculated Bulk Elastic Properties for the $Fe-Cr_{12}-Si_2$[a]

	B	E	G	ν
present work	203	228	86	0.31
exp.[48]	157	178	68	0.31

[a]The different elastic moduli are given in GPa while ν is unitless.

Many variables affect the gap between MD and experimental results, for example, a limited simulation box size of a few nm, impurity densities, grain boundaries and other defects present in physical samples, and finally, the environmental conditions of the experiments. Despite these limitations, the calculated elastic properties using our MEAM potential are in good agreement with the experimental values. This difference is constant for the elastic moduli, so the relationship between the elastic properties is maintained, which is reflected in the Poisson's ratio obtained for the perfect crystal. The LAMMPS potential file created with our obtained parameters and associated input files are available in the Supporting Information. Figure 1 shows the stress−strain response of a pure Fe sample at 300 K with a strain rate of 10^{-3} Å/ps as a function of different potentials. Here, we can see from Figure 1 that the Bonny's[49] potential leads to the highest ultimate strength (~25 GPa) among all the potentials, whereas our

https://doi.org/10.1021/acs.jpcc.1c07021
J. Phys. Chem. C 2021, 125, 22863−22871

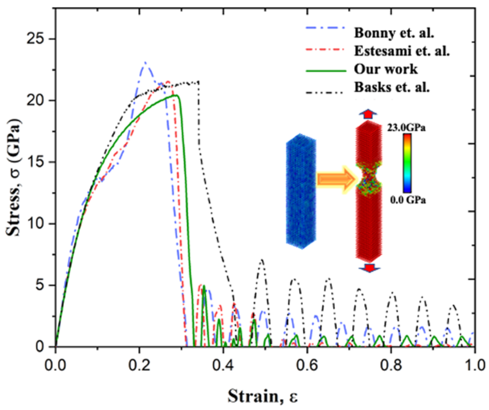

Figure 1. Stress−strain curve with a 10^{-3} Å/ps strain rate at 300 K simulated using three other different interatomic potentials and our developed MEAM potential for Fe-Fe interactions.

MEAM potential leads to the lowest (~20 GPa), which is 20% lower than the highest one.

The ultimate strength of Fe for all other potentials[21,50] stays in this ±5 GPa band, and therefore, we can conclude that the stress−strain behavior for our developed MEAM potential is very close to other established Fe forcefields. Furthermore, we have seen that the stress−strain behavior for Cr and Si has a good agreement with previously developed potentials (see the Supporting Information).

4. STRUCTURAL AND THERMAL PROPERTIES

The structural parameters have been analyzed by investigating the radial distribution function (RDF) for different potentials and literature values. We have evaluated the RDF for Fe-Fe, Fe-Cr, and Fe-Si pairs determined by our parameterized MEAM potential by comparing them with previously calculated RDF values using the DFT approach and other MD forcefields.[51,52] The mathematical expression for the calculation of RDF will be as follows[53]

$$g(r) = \frac{V}{N^2}\frac{\sum_{i=1}^{N_i} n_i(r)}{4\pi r^2 \mathrm{d}r} \quad (2)$$

Here, V is the cell volume, and N is the number of atoms in the cell. The atomic number function is defined as $n_i(r)$ from radius r to $r + \mathrm{d}r$, and N_i can be defined as the number of neighboring atoms around the ith atom in the system. In Figure 2, we have shown a comparison of the RDF between our calculated values and different literature values. The RDF for different atomic pairs has been calculated in $Fe_{92}Cr_8$ and $Fe_{92}Si_8$ at 1.0 atmospheric pressure and 3100 K temperature to see how well our parameterized MEAM forcefield can describe atomic interactions at the liquid phase of the material.

Figure 2a shows the comparison of RDF for $Fe_{92}Si_8$ with a density of 5.90 g/cm^3, calculated using our MEAM potential and another MEAM potential by Aslam et al.[54] Also, RDF data from the previous ab initio[51] calculation have been included in this comparison. In a previous study,[51] the RDF is calculated using the First Principle (FP)-MD method under the same conditions as here, where their calculated values roughly matched with the previous studies.[55−57] Figure 2a shows that the first and second peaks for Fe-Si pairs are located at ~2.3 and ~4.5 Å, respectively, for all the potentials and literature values. Moreover, in Figure 2b, we can see that for Fe-Cr with a density of 9.38 g/cm^3, the first $g(r)$ peak appeared at the position of ~2.4 Å and the second peak at ~4.5 Å, which is almost the same as the values reported in a previous study.[51]

We also utilized this potential to determine thermal properties and fitted them against the values calculated using other established potentials for individual elements. We did not find any thermal property values for the Fe-Cr-Si alloy combination in previous studies. Figure 3 shows a comparison between the thermal expansion behavior for unary crystals calculated using our MEAM potential and other potentials as a function of temperature. In Figure 3a, we have calculated the linear thermal expansion percentage for Fe, which matches the values reported in a previous study.[58] We also calculated the thermal expansion for the $Fe_{86}Cr_{12}Si_2$ composite, Figure 3a, showing a lower thermal expansion than the pure iron. The high oxidation resistance of $Fe_{86}Cr_{12}Si_2$ even at elevated temperatures[59] and the fact that composite alloys with lower oxidation tendency show lower thermal expansion can be explained.[60] Figure 3b,c show the comparison of the thermal expansion coefficient (TEC), calculated using different potentials[61,62] and our parameterized MEAM potential for

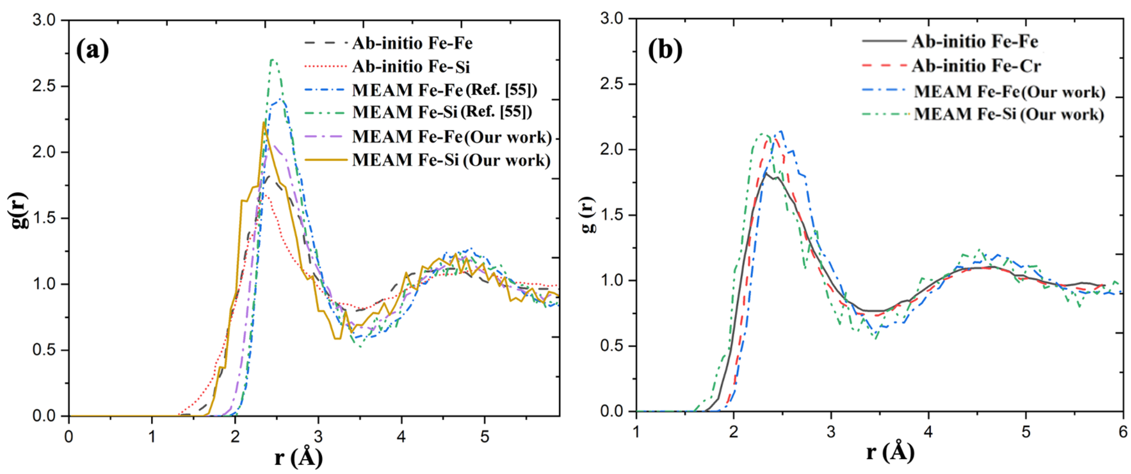

Figure 2. Radial distribution functions for (a) $Fe_{92}Si_8$ and (b) $Fe_{92}Cr_8$ at 1 bar with 3100 K; the RDF has been calculated using MEAM potentials (one parameterized in the present study and the other parameterized by Aslam et al.[54]) using MD simulation. The ab initio calculated data have been taken from the literature by Posner et al.[51]

https://doi.org/10.1021/acs.jpcc.1c07021
J. Phys. Chem. C 2021, 125, 22863−22871

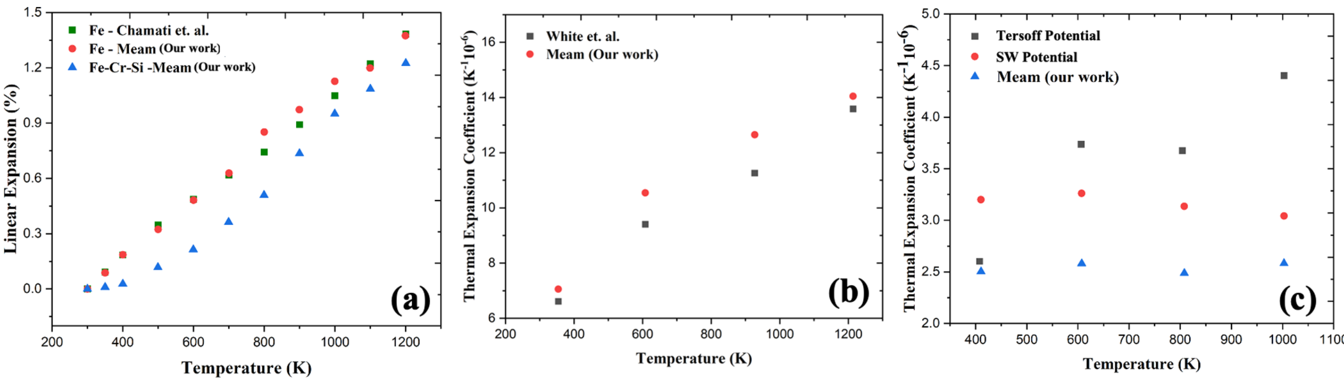

Figure 3. Thermal expansion benchmarking; (a) linear thermal expansion of BCC-Fe relative to 300 K (room temperature) calculated by the proposed MEAM potential compared the reported literature values;[58] comparison of the TEC of Cr (b) and Si (c) for different potentials.

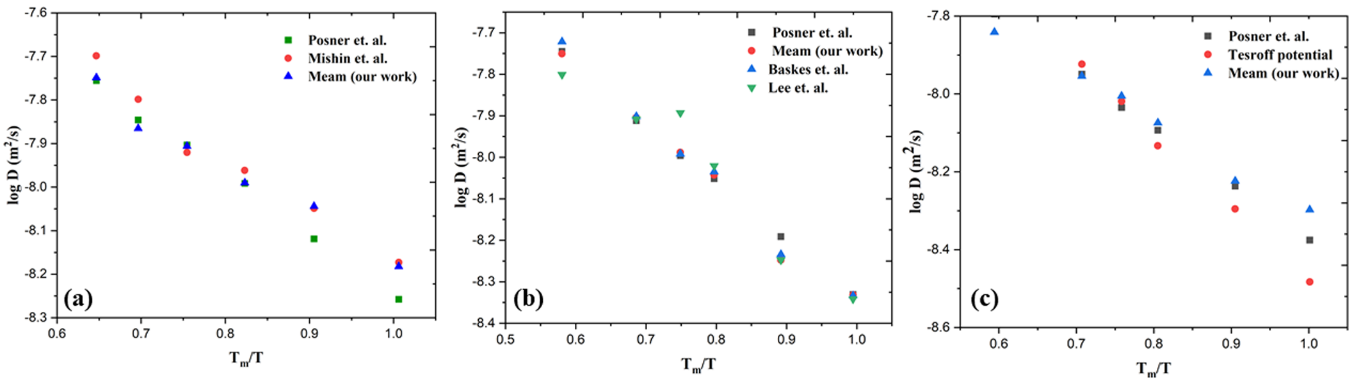

Figure 4. Thermal diffusion coefficient of (a) Fe, (b) Cr, and (c) Si; calculated using different interatomic potentials (including the proposed MEAM potential that we have parameterized in this study) and literature data at 1.0 atm as a function of the inverse of the homologous temperature ($T_h^{-1} = T/T_m$) to make comparison with the values calculated using our potential.

the other two components Si and Cr. Our developed MEAM potential TEC values matched very closely with the values reported in the previous study[62] for Cr, Figure 3b. The TEC values for Si[61] calculated using the Tersoff[63] and Stillinger-Weber (SW)[64] potentials closely match the experimental values reported in previous studies.[65,66] Figure 3c shows a close match between the TEC values predicted by our developed MEAM and the values calculated using Tersoff and SW potentials.

We calculated the thermal self-diffusion for Fe, Cr, and Si crystals for our MEAM potential at 1.0 atm pressure as a function of homologous temperature, $T_h = T/T_m$, where T_m is the melting temperature and T is the system temperature. The Arrhenius equation expresses thermal diffusion

$$D = D_h \exp(-gT_h) \tag{3}$$

Here, activation constant, g, and yielding constant diffusivity, D_h, are empirical numbers. The diffusion coefficient calculated using our proposed MEAM potential closely matches the other potentials[18,21,63] and literature values, Figure 4. Previous studies reported $\sim 4 \times 10^{-9}$ m^2/s as the constant diffusivity along the melting curve[51,57] for Si and Cr, and $\sim 5 \times 10^{-9}$ m^2/s for Fe. These values closely match what we calculated ($\sim 5.5 \times 10^{-9}$ m^2/s for Fe, referring to Figure 4a; $\sim 4 \times 10^{-9}$ m^2/s for Cr and Si, referring to Figure 4b,c along the melting curve). The activation constant, g, calculated using our potential, also matches the values reported in a previous study ($\sim$3.0).[67]

5. FINITE TEMPERATURE STRUCTURAL STABILITY TESTS

We examined the thermal and kinetic behavior of the Fe-Cr-Si alloy system. To verify our potential parameters at a nonzero temperature, we considered a system of 16,000 atoms with the stoichiometry of $Fe_{86}-Cr_{12}-Si_2$. Initially, we relaxed the structure at room temperature, 300 K, in the NVT ensemble for 200 ps with 1 fs timesteps. The structure remained crystalline as we relaxed with our proposed MEAM forcefield at 300 K, Figure 5a, which has further been proved by comparing the coordinates of the $Fe_{86}Cr_{12}Si_2$ alloy system at room temperature and 0 K, Figure 5b. The first and second significant peaks are at a distance of 2.5 and 4.8 Å, demonstrating the proposed potential's capability for describing the Fe-Cr-Si system for nonzero temperatures.

Moreover, Figure 5c depicts the temperature variations throughout the NVT relaxation process with the simulation time, which converges to the set temperature for a long-enough simulation. Figure 5d shows the total energy as a function of the simulation time in the NVE ensemble at 0 and 300 K that converge.

6. CONCLUSIONS

We developed a MEAM interatomic potential for the Fe-Cr-Si's ternary alloy system and fitted the potential for different urinary and binary metallic interactions. We validated our potential by comparing the calculated material properties with values reported in the literature for ab initio calculations and experimental measurements. Although the MEAM potential

https://doi.org/10.1021/acs.jpcc.1c07021
J. Phys. Chem. C 2021, 125, 22863−22871

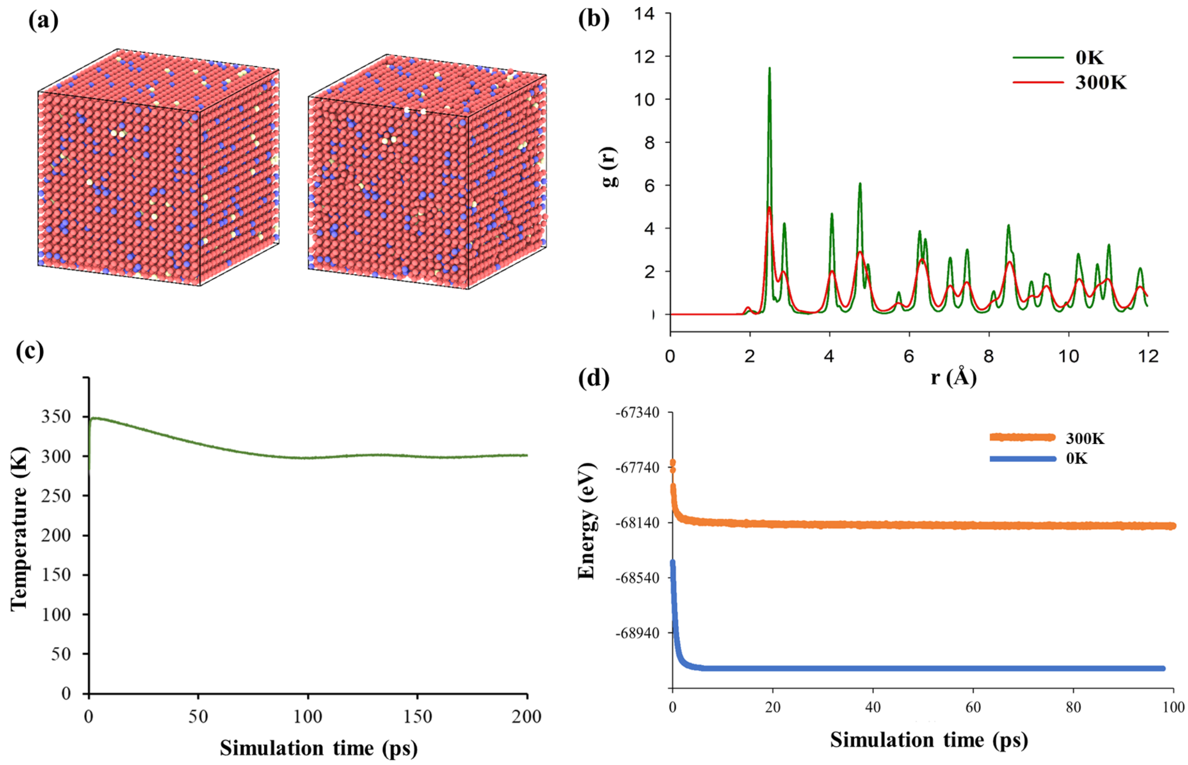

Figure 5. Finite temperature stability test of the developed MEAM forcefield for the Fe-Cr-Si system ($Fe_{86}Cr_{12}Si_2$); (a) Initial and relaxed structure under the NVT ensemble at 300 K for the specified concentration of the Fe, Cr, and Si system; (b) coordination analysis for the relaxed structure at 0 and 300 K temperatures; (c) relaxation curve for the Fe-Cr-Si system at 300 K with the simulation time; and (d) total energy variation of the NVE ensemble at the temperature of 0 and 300 K.

cannot describe the ionic charge-induced or long-range interactions, the proposed potential can describe the mechanical and thermodynamic behavior of the Fe-Cr-Si system. The predicted properties using our developed potential are in good agreement with DFT and experimental calculations, falling in the observed ranges. The correct reproduction of the substitutional and vacancy formation energies is expected to adequately describe the diffusive behavior when subjected to thermal and irradiation effects (Supporting Information).

We tested the ternary potential at both zero and nonzero temperatures by modeling the bulk $Fe_{86}Cr_{12}Si_2$ alloy, indicating the integrity of the crystal at room temperature. Moreover, the bulk elastic properties were measured, describing close values to experimental values. Our potential is capable of reproducing the intended interaction profile for both unary and binary relations. The Fe-Cr system that is alloyed with other materials has implications in nuclear reactors and materials that need to operate at elevated temperatures and corrosive environments. In this case, we have used silicon with the Fe-Cr system. The proposed potential has various applications, for example, the design of multimetallic layered composites for extreme temperatures and radiation doses.

■ ASSOCIATED CONTENT

Supporting Information

The Supporting Information is available free of charge at https://pubs.acs.org/doi/10.1021/acs.jpcc.1c07021.

Theoretical formulation of the MEAM potential, that is, unary and multibody functions parameters, stress−strain plots of Si and Cr, defect formation energy validation, and the LAMMPS potential file. (PDF)

The LAMMPS potential file (ZIP)

■ AUTHOR INFORMATION

Corresponding Author

Kasra Momeni − *Department of Mechanical Engineering, University of Alabama, Tuscaloosa, Alabama 35487, United States;* orcid.org/0000-0002-4209-1129; Email: kmomeni@ua.edu

Authors

Shiddartha Paul − *Department of Mechanical Engineering, University of Alabama, Tuscaloosa, Alabama 35487, United States;* orcid.org/0000-0003-4306-180X

Mario Muralles − *School of Materials Science and Engineering, Nanyang Technological University, 639798, Singapore*

Daniel Schwen − *Department of Computational Mechanics and Materials, Idaho National Laboratory, Idaho Falls, Idaho 83402, United States*

Michael Short − *Department of Nuclear Science & Engineering, Massachusetts Institute of Technology, Cambridge, Massachusetts 02139, United States;* orcid.org/0000-0002-9216-2482

Complete contact information is available at: https://pubs.acs.org/10.1021/acs.jpcc.1c07021

Notes

The authors declare no competing financial interest.
All data obtained during this project are available from the authors.

https://doi.org/10.1021/acs.jpcc.1c07021
J. Phys. Chem. C 2021, 125, 22863−22871

■ ACKNOWLEDGMENTS

This project is partly supported by DoE-ARPA-E OPEN (DE-AR0001066) and the NSF-CAREER under NSF cooperative agreement CBET-2042683.

■ REFERENCES

(1) Fetni, S.; Toumi, A.; Mkaouar, I.; Boubahri, C.; Briki, J. Microstructure Evolution and Corrosion Behaviour of an ASTM A213 T91 Tube after Long Term Creep Exposure. *Eng. Fail. Anal.* **2017**, *79*, 575−591.

(2) Shi, Z.; Cao, J.; Han, F. Preparation and Characterization of Fe−Al Intermetallic Layer on the Surface of T91 Heat-Resistant Steel. *J. Nucl. Mater.* **2014**, *447*, 77−81.

(3) Wang, Z. Finite Element Analysis of Residual Stress in Welded Joints of T91 Steel. *IOP. Conf. Ser.: Mater. Sci. Eng.* **2019**, *637*, 12013.

(4) Gong, Y.; Yang, Z.-G.; Yang, F.-Y. Heat Strength Evaluation and Microstructures Observation of the Welded Joints of One China-Made T91 Steel. *J. Mater. Eng. Perform.* **2012**, *21*, 1313−1319.

(5) Terrani, K. A.; Zinkle, S. J.; Snead, L. L. Advanced Oxidation-Resistant Iron-Based Alloys for LWR Fuel Cladding Q. *J. Nucl. Mater.* **2014**, *448*, 420−435.

(6) Pint, B. A.; Terrani, K. A.; Brady, M. P.; Cheng, T.; Keiser, J. R. High Temperature Oxidation of Fuel Cladding Candidate Materials in Steam − Hydrogen Environments Q. *J. Nucl. Mater.* **2013**, *440*, 420−427.

(7) Gigax, J. G.; Chen, T.; Kim, H.; Wang, J.; Price, L. M.; Aydogan, E.; Maloy, S. A.; Schreiber, D. K.; Toloczko, M. B.; Garner, F. A.; Shao, L. Radiation Response of Alloy T91 at Damage Levels up to 1000 Peak Dpa. *J. Nucl. Mater.* **2016**, *482*, 257−265.

(8) Kuksenko, V.; Pareige, C.; Genevois, C.; Pareige, P. Characterisation of Cr, Si and P Distribution at Dislocations and Grain-Boundaries in Neutron Irradiated Fe-Cr Model Alloys of Low Purity. *J. Nucl. Mater.* **2013**, *434*, 49−55.

(9) Lu, Z.; Faulkner, R. G.; Was, G.; Wirth, B. D. Irradiation-Induced Grain Boundary Chromium Microchemistry in High Alloy Ferritic Steels. *Scr. Mater.* **2008**, *58*, 878−881.

(10) Moona, J.; Kima, S.; Kimb, J. H.; Shortc, M. P.; Bahna, C. B. Oxidation Resistance Evaluation of FeCrSi Alloy in High Temperature Steam Environment. In *Transactions of the Korean Nuclear Society Spring Meeting, Jeju, Korea*; Korean Nuclear Society, Daejeon, Republic of Korea: Jeju, Korea, 2018.

(11) Qiang, R.; Leong, A.; Zhang, J.; Short, M. P. Corrosion Behavior of Fe−Cr−Si Alloys in Simulated PWR Primary Water Environment. *J. Nucl. Mater.* **2019**, *526*, 151735.

(12) Paul, S.; Schwen, D.; Short, M. P.; Momeni, K. Effect of Irradiation on Ni-Inconel/Incoloy Heterostructures in Multimetallic Layered Composites. *J. Nucl. Mater.* **2021**, *547*, No. 152778.

(13) Lee, B. J.; Baskes, M. I. Second Nearest-Neighbor Modified Embedded-Atom-Method Potential. *Phys. Rev. B* **2000**, *62*, 8564−8567.

(14) Liu, P.; Han, X.; Sun, D.; Wang, Q. Development and Application of a Ternary Ti-Al-N Interatomic Potential for Ti2AlN/TiAl Composite. *J. Alloys Compd.* **2018**, *745*, 63−74.

(15) Ding, S.; Wang, X. A Systematic Study on the MEAM Interatomic Potentials of the Transition Metal Nitrides TMNs (TM=Ti, V, Cr, Fe) Binary Systems. *J. Alloys Compd.* **2019**, *805*, 1081−1089.

(16) Choi, W.-M.; Jo, Y. H.; Sohn, S. S.; Lee, S.; Lee, B.-J. Understanding the Physical Metallurgy of the CoCrFeMnNi High-Entropy Alloy: An Atomistic Simulation Study. *npj Comput. Mater.* **2018**, *4*, 1−9.

(17) Lin, Y.; Yang, T.; Lang, L.; Shan, C.; Deng, H.; Hu, W.; Gao, F. Enhanced Radiation Tolerance of the Ni-Co-Cr-Fe High-Entropy Alloy as Revealed from Primary Damage. *Acta Mater.* **2020**, *196*, 133.

(18) Choi, W. M.; Kim, Y.; Seol, D.; Lee, B. J. Modified Embedded-Atom Method Interatomic Potentials for the Co-Cr, Co-Fe, Co-Mn, Cr-Mn and Mn-Ni Binary Systems. *Comput. Mater. Sci.* **2017**, *130*, 121−129.

(19) Jelinek, B.; Groh, S.; Horstemeyer, M. F.; Houze, J.; Kim, S.-G.; Wagner, G. J.; Moitra, A.; Baskes, M. I. Modified Embedded Atom Method Potential for Al, Si, Mg, Cu, and Fe Alloys. *Phys. Rev. B* **2012**, *85*, No. 245102.

(20) Rose, J. H.; Smith, J. R.; Guinea, F.; Ferrante, J. Universal Features of the Equation of State of Metals. *Phys. Rev. B* **1984**, *29*, 2963.

(21) Lee, B.-J.; Baskes, M. I.; Kim, H.; Koo Cho, Y. Second Nearest-Neighbor Modified Embedded Atom Method Potentials for Bcc Transition Metals. *Phys. Rev. B* **2001**, *64*, No. 184102.

(22) Baskes, M. I. Modified Embedded-Atom Potentials for Cubic Materials and Impurities. *Phys. Rev. B* **1992**, *46*, 2727−2742.

(23) Hestenes, M. R.; Stiefel, E. Methods of Conjugate Gradients for Solving Linear Systems. *J. Res. Natl. Bur. Stan.* **1952**, *49*, 409−436.

(24) Plimpton, S.; Crozier, P.; Thompson, A. LAMMPS-Large-Scale Atomic/Molecular Massively Parallel Simulator. *Sandia Natl. Lab.* **2007**, *18*, 43.

(25) Kim, S. G.; Horstemeyer, M. F.; Baskes, M. I.; Rais-Rohani, M.; Kim, S.; Jelinek, B.; Houze, J.; Moitra, A.; Liyanage, L. Semi-Empirical Potential Methods for Atomistic Simulations of Metals and Their Construction Procedures. *J. Eng. Mater. Technol.* **2009**, *131*, No. 041210.

(26) Chen, H.-L.; Su, C.-H.; Ju, S.-P.; Liu, S.-H.; Chen, H.-T. Local Structural Evolution of Fe 54 C 18 Cr 16 Mo 12 Bulk Metallic Glass during Tensile Deformation and a Temperature Elevation Process: A Molecular Dynamics Study. *RSC Adv.* **2015**, *5*, 103925−103935.

(27) Simmons, G.; Wang, H. *Single Crystal Elastic Constants and Calculated Aggregate Properties: A Handbook 2nd Ed*; MIT Press: Cambridge, Mass, 1971, 370.

(28) Ryu, S.; Weinberger, C. R.; Baskes, M. I.; Cai, W. Improved Modified Embedded-Atom Method Potentials for Gold and Silicon. *Modelling Simul. Mater. Sci. Eng.* **2009**, *17*, No. 075008.

(29) Schall, J. D.; Gao, G.; Harrison, J. A. Elastic Constants of Silicon Materials Calculated as a Function of Temperature Using a Parametrization of the Second-Generation Reactive Empirical Bond-Order Potential. *Phys. Rev. B* **2008**, *77*, No. 115209.

(30) Lee, B.; Rudd, R. E. First-Principles Calculation of Mechanical Properties of Si< 001> Nanowires and Comparison to Nano-mechanical Theory. *Phys. Rev. B* **2007**, *75*, No. 195328.

(31) Dobbs, E. R. Equation of State and Elasticity of Solid Argon. *J. Chem. Phys.* **1956**, *24*, 477−478.

(32) Petrova, A. E.; Krasnorussky, V. N.; Stishov, S. M. Elastic Properties of FeSi. *J. Exp. Theor. Phys.* **2010**, *111*, 427−430.

(33) Acun, A. D.; Soyalp, F. Elastic and Phonon Properties of FeSi and CoSi in the B2 Structure. *Philos. Mag.* **2012**, *92*, 635−646.

(34) Okamoto, H. Cr-Si (Chromium-Silicon). *J. Phase Equilibria* **2001**, 593.

(35) Moroni, E. G.; Wolf, W.; Hafner, J.; Podloucky, R. Cohesive, Structural, and Electronic Properties of Fe-Si Compounds. *Phys. Rev. B* **1999**, *59*, 12860−12871.

(36) Ren, B.; Lu, D.-H.; Zhou, R.; Ji, D.-P.; Hu, M.-Y.; Feng, J. First Principles Study of Stability, Mechanical, and Electronic Properties of Chromium Silicides. *Chin. Phys. B* **2018**, *27*, No. 107102.

(37) Zinoveva, G. P.; Andreeva, L. P.; Geld, P. V. Elastic Constants and Dynamics of Crystal Lattice in Monosilicides with B20 Structure. *Phys. Status Solidi* **1974**, *23*, 711−718.

(38) Zhang, H.; Wang, G.; Punkkinen, M. P. J.; Hertzman, S.; Johansson, B.; Vitos, L. Elastic Anomalies in Fe-Cr Alloys. *J. Phys. Condens. Matter* **2013**, *25*, No. 195501.

(39) Ruban, A. V.; Razumovskiy, V. I. First-Principles Based Thermodynamic Model of Phase Equilibria in Bcc Fe-Cr Alloys. *Phys. Rev. B* **2012**, *86*, No. 174111.

(40) Mishra, R. S.; Nene, S. S.; Frank, M.; Sinha, S.; Liu, K.; Shukla, S. Metastability Driven Hierarchical Microstructural Engineering: Overview of Mechanical Properties of Metastable Complex Concentrated Alloys. *J. Alloys Compd.* **2020**, *842*, No. 155625.

(41) Pan, Y.; Pu, D. L.; Yu, E. D. Structural, Electronic, Mechanical and Thermodynamic Properties of Cr−Si Binary Silicides from First-Principles Investigations. *Vacuum* **2021**, *185*, No. 110024.

(42) de Jong, M.; Chen, W.; Angsten, T.; Jain, A.; Notestine, R.; Gamst, A.; Sluiter, M.; Krishna Ande, C.; van der Zwaag, S.; Plata, J. J.; Toher, C.; Curtarolo, S.; Ceder, G.; Persson, K. A.; Asta, M. Charting the Complete Elastic Properties of Inorganic Crystalline Compounds. *Sci. Data* **2015**, *2*, 150009.
(43) Errandonea, D.; Santamaría-Perez, D.; Vegas, A.; Nuss, J.; Jansen, M.; Rodríguez-Hernandez, P.; Muñoz, A. Structural Stability of Fe5 Si3 and Ni2 Si Studied by High-Pressure x-Ray Diffraction and Ab Initio Total-Energy Calculations. *Phys. Rev. B* **2008**, *77*, No. 094113.
(44) Zaleski, P.; Szymański, K.; Przewoźnik, J.; Rećko, K.; Cottrell, S.; Dobrzyński, L. Cr3Si Doped by Co Studied by Muon Spin Relaxation and Scanning Electron Microscopy Techniques. *J. Alloys Compd.* **2010**, *498*, 5−12.
(45) Dauben, C. H.; Templeton, D. H.; Myers, C. The Crystal Structure Of Cr5Si3. *J. Phys. Chem.* **1956**, *60*, 443−445.
(46) Zhu, H.; Shi, L.; Li, S.; Zhang, S.; Xia, W. Effects of Biaxial Strains on Electronic and Elastic Properties of Hexagonal XSi2 (X = Cr, Mo, W) from First-Principles. *Solid State Commun.* **2018**, *270*, 99−106.
(47) Hill, R. The Elastic Behaviour of a Crystalline Aggregate. *Proc. Phys. Soc. A* **1952**, *65*, 349−354.
(48) Lee, J.; Kim, T.; Hwang, I. S.; Ballinger, R. G.; Kim, J. H. Development of Pilgering Process of Hybrid-Layer Cladding for Advanced Small Modular Fast Reactor Application. *Int. Conf. Fast React. Relat. Fuel Cycles* **2017**, 1−10.
(49) Bonny, G.; Castin, N.; Terentyev, D. Interatomic Potential for Studying Ageing under Irradiation in Stainless Steels: The FeNiCr Model Alloy. *Modelling Simul. Mater. Sci. Eng.* **2013**, *21*, No. 085004.
(50) Etesami, S. A.; Asadi, E. Molecular Dynamics for near Melting Temperatures Simulations of Metals Using Modified Embedded-Atom Method. *J. Phys. Chem. Solids* **2018**, *112*, 61−72.
(51) Posner, E. S.; Rubie, D. C.; Frost, D. J.; Vlček, V.; Steinle-Neumann, G. High P−T Experiments and First Principles Calculations of the Diffusion of Si and Cr in Liquid Iron. *Geochim. Cosmochim. Acta* **2017**, *203*, 323−342.
(52) Zhou, X. W.; Foster, M. E.; Sills, R. B. An Fe-Ni-Cr Embedded Atom Method Potential for Austenitic and Ferritic Systems: An Fe-Ni-Cr Embedded Atom Method Potential for Austenitic and Ferritic Systems. *J. Comput. Chem.* **2018**, *39*, 2420−2431.
(53) Zhang, X.; Li, B.; Liu, H. X.; Zhao, G. H.; Yang, Q. L.; Cheng, X. M.; Wong, C. H.; Zhang, Y. M.; Lim, C. W. J. Atomic Simulation of Melting and Surface Segregation of Ternary Fe-Ni-Cr Nanoparticles. *Appl. Surf. Sci.* **2019**, *465*, 871−879.
(54) Aslam, I.; Baskes, M. I.; Dickel, D. E.; Adibi, S.; Li, B.; Rhee, H.; Asle Zaeem, M.; Horstemeyer, M. F. Thermodynamic and Kinetic Behavior of Low-Alloy Steels: An Atomic Level Study Using an Fe-Mn-Si-C Modified Embedded Atom Method (MEAM) Potential. *Materialia* **2019**, *8*, No. 100473.
(55) Morard, G.; Andrault, D.; Antonangeli, D.; Bouchet, J. Properties of Iron Alloys under the Earth's Core Conditions. *Comptes Rendus Geosci.* **2014**, *346*, 130−139.
(56) Alfè, D.; Gillan, M. J.; Price, G. D. Composition and Temperature of the Earth's Core Constrained by Combining Ab Initio Calculations and Seismic Data. *Earth Planet. Sci. Lett.* **2002**, *195*, 91−98.
(57) Pozzo, M.; Davies, C.; Gubbins, D.; Alfè, D. Transport Properties for Liquid Silicon-Oxygen-Iron Mixtures at Earth's Core Conditions. *Phys. Rev. B* **2013**, *87*, 14110.
(58) Chamati, H.; Papanicolaou, N. I.; Mishin, Y.; Papaconstantopoulos, D. A. Embedded-Atom Potential for Fe and Its Application to Self-Diffusion on Fe(100). *Surf. Sci.* **2006**, *600*, 1793−1803.
(59) Leong, A.; Yang, Q.; McAlpine, S. W.; Short, M. P.; Zhang, J. Oxidation Behavior of Fe-Cr-2Si Alloys in High Temperature Steam. *Corros. Sci.* **2021**, *179*, No. 109114.
(60) Haynes, J. A.; Pint, B. A.; Porter, W. D.; Wright, I. G. Comparison of Thermal Expansion and Oxidation Behavior of Various High-Temperature Coating Materials and Superalloys. *Mater. High Temp.* **2004**, *21*, 87−94.
(61) Nejat Pishkenari, H.; Mohagheghian, E.; Rasouli, A. Molecular Dynamics Study of the Thermal Expansion Coefficient of Silicon. *Phys. Lett. A* **2016**, *380*, 4039−4043.
(62) White, G. K.; Andrikidis, C. Thermal Expansion of Chromium at High Temperature. *Phys. Rev. B* **1996**, *53*, 8145.
(63) Tersoff, J. Empirical Interatomic Potential for Silicon with Improved Elastic Properties. *Phys. Rev. B* **1988**, *38*, 9902.
(64) Stillinger, F. H.; Weber, T. A. Computer Simulation of Local Order in Condensed Phases of Silicon. *Phys. Rev. B* **1985**, *31*, 5262.
(65) Watanabe, H.; Yamada, N.; Okaji, M. Linear Thermal Expansion Coefficient of Silicon from 293 to 1000 K. *Int. J. Thermophys.* **2004**, *25*, 221−236.
(66) Yim, W. M.; Paff, R. J. Thermal Expansion of AlN, Sapphire, and Silicon. *J. Appl. Phys.* **1974**, *45*, 1456−1457.
(67) Saxton, H. J.; Sherby, O. D. Viscosity and Atomic Mobility in Liquid Metals. *Am. Soc. Metals Trans. Quart.* **1962**, *55*, 4756511.

https://doi.org/10.1021/acs.jpcc.1c07021
J. Phys. Chem. C 2021, 125, 22863−22871